



Transient Stability of Multi-Machine Wind Turbine Generators System Connected to the Power Network

Ayat Y. Elsharif¹, Elfadil Z. Yahia², Kamal R. Doud³

¹Department of Electrical Engineering, Collage of Engineering, Sudan International University
Khartoum, Sudan (E-mail: e-ayat1284@hotmail.com)

²School of Electrical and Nuclear Engineering, Collage of Engineering, Sudan University of Science and Technology
Khartoum, Sudan (E-mail: fzy17077@gmail.com)

³Department of Electrical and Electronics Engineering, Faculty of Engineering University of Khartoum
Khartoum, Sudan (E-mail: kamalramdam@uofk.edu)

Abstract: currently worldwide installed capacity of the network connected wind generators grows rapidly; this rise of integration rate of wind energy could lead to circulation of transient stability and could potentially cause local or system wide blackout. This paper presents a recovery strategy that enables the system of HVDC transmission systems based on voltage source converter, which transmit electrical power from the wind turbines to the power network, to ride-through different positions of ac faults with smallest amount current and voltage stresses on the converter switching devices. Issue such as control strategies for a VSC-HVDC conduction system connecting offshore wind farms to the power network is discussed. The results show that the transient stability study of the system is widely different when the faults occur in neither wind side nor power network side. The DC link voltage behaves similarly to the AC voltage. However when the AC fault occurs in the wind side stations either for ac voltage or DC voltage the system behavior does not return to its normal operation after the fault is cleared. A reduced network model has been implemented in MATLAB/ SIMULINK to assess control performance during the fault.

Keywords: High voltage; Direct current transmission; Voltage source converter (VSC); Off shore wind farms.

1. INTRODUCTION

Multi-terminal HVDC (MTDC) systems have been proposed for transmitting power between conventional ac networks and connecting wind farms. It has been identified that large wind farms can potentially provide significant contributions to transmission set of connections operation, e.g., frequency regulation, power system stabilization [1].

The principle characteristics of VSC transmission are that no external voltage source for commutation is required, it can independently control the imprudent power flow at each AC network, and reactive power control is independent of the active power control. These features make VSC transmission attractive for connection of weak AC systems, island networks and renewable sources to a main grid.

The four currently most used wind turbine generator technologies in large-scale wind farm installations worldwide are Fixed' speed induction generators (FSIG). Small speed range wound rotor induction generators, Variable speed especially fed induction generators (DFIG) and Variable speed series converter-connected generators [2].

The wind power system consists of one or more units, operating electrically in parallel. Because of the large moment of inertia of the rotor, the blueprint challenges include the starting, the speed control during the power producing process and stopping the turbine when required [3]. The strategy for controlling the speed of the wind turbine varies with the type of the electrical machine used dc machine, synchronous or induction machine.

The disadvantages of both the DC contraption and the synchronous machine are eliminated in the induction machine, resulting in low capital cost, low preservation, and better transient presentation. For these reasons, the induction generator is extensively used in miniature and bulky wind farms and small hydroelectric power plants [3].

When a short circuit fault occurs at or in the neighborhood of the generator terminals, the machine significantly contributes to the system fault current, particularly if it is successively on light load. The short circuit current is always more severe for a single-phase fault than a three-phase fault. The most important quantity is the first peak current as it determines the rating of the protective circuit breaker needed

to protect the generator against many faults. The short circuit current has a slowly decaying *DC* component, and an *AC* component. The concluding is larger than the direct on-line starting inrush current, and may reach 10-15 times the full load rated current [3]. This can be clearly noticed in the results.

2. SYSTEM OUTLINE

Fig. 1 shows the single line diagram of proposed test system. It consists of two wind farm rated at 33KV, 750MVA based on doubly-fed induction generator wind turbines with pitch control. The *DC* transmission system in Fig. 1 is arranged in bi-polar form to progress system pliability against single-pole to ground faults. The converters *VSC*₁ to *VSC*₄ are controlled with sinusoidal pulse width modulation (*SPWM*) using 2.1 kHz switching frequency. Converters *VSC*₁ and *VSC*₃ regulates the active power and *ac* voltage magnitude at buses *B*₁ and *B*₃. Converters *VSC*₂ and *VSC*₄ regulates the *DC* link voltage and *AC* voltage magnitude at buses *B*₂ and *B*₄. The *AC* harmonic filters are used to eliminate and reduce high order harmonic generated in the converters and a 2310μ*F* capacitors are used in the *DC* link. The distance between the stations is 120 *km* and the conduction voltage is ±150 *kV*. The ratings of the synchronous machines *SG*₁ and *SG*₂ are 230 *kV* and 1400 *MVA* at 50 *Hz* [4,5].

3. SYSTEM MODELING

A. Operator reactance and parameters of double-cage or deep-bar rotor of the induction machine

The *dq* model of a doubly fed induction generator with a wound rotor is similar to the model of an induction motor. For both double-cage and deep-bar rotors, assumed that the end-rings resistance and the part of the leakage flux which links the two rotor windings, but not the stator, are neglected. Therefore, both rotor types are represented by two parallel rotor circuits as shown in the operational equivalent circuit of Fig. 2(a)[2].

The corresponding steady state equivalent circuit is shown in Fig. 2(b). As shows in Fig. 2(c) an alternative steady state equivalent circuit where the two rotor branches are converted into a single equivalent branch whose resistance and reactance are functions of motor slip *s* as follows [2].

$$R_{(r)}(s) = \frac{R_{r1}R_{r2}(R_{r1}+R_{r2})+s^2(R_{r2}X_{or1}^2+R_{r1}X_{or2}^2)}{(R_{r1}+R_{r2})^2+s^2(X_{or1}+X_{or2})^2} \quad (1)$$

$$X_{(r)}(s) = \frac{X_{or2}R_{r1}^2+X_{or1}R_{r2}^2+s^2X_{or1}X_{or2}(X_{or1}+X_{or2})}{(R_{r1}+R_{r2})^2+s^2(X_{or1}+X_{or2})^2} \quad (2)$$

From the operational circuit of Fig. 2(a), and as in the case of a single rotor winding, the complex form of the motor voltage and flux linkage equations can be written by inspection as follows:

$$V_s = p\psi_s + j\omega_r\psi_s + R_s I_s \quad (3)$$

$$0 = R_{r1}I_{r1} + p\psi_{r1} \quad (4)$$

$$0 = R_{r2}I_{r2} + p\psi_{r2} \quad (5)$$

where

$$\psi_s = (L_{os} + L_m)I_s + L_m I_{r1} + L_m I_{r2} \quad (6)$$

$$\psi_{r1} = L_m I_s + (L_{or1} + L_m)I_{r1} + L_m I_{r2} \quad (7)$$

$$\psi_{r2} = L_m I_s + L_m I_{r1} + (L_{or2} + L_m)I_{r2} \quad (8)$$

The derivation of the operational reactance is similar to that in the case of a single rotor winding except that more algebra is involved. The steps are summarized as follows: substitute Equation (7) in Equation (4), Equation (8) in Equation (5), eliminate *I*_s and express *I*_{r1} in terms of *I*_{r2}, express *I*_{r1} and *I*_{r2} in terms of *I*_s and substitute these results back in Equation (6). It can be shown that the result is given by

$$\frac{\psi_s}{I_s} = (L_{os} + L_m) - \frac{H}{D}$$

where: $H = L_m^2(R_{r1} + R_{r2})p + L_m^2(L_{or1} + L_{or2})p^2$

$D = R_{r1}R_{r2} + [R_{r1}(L_{or2} + L_m) + R_{r2}(L_{or1} + L_m)]p + [L_{or1}L_m + L_{or2}(L_{or1} + L_m)]p^2$

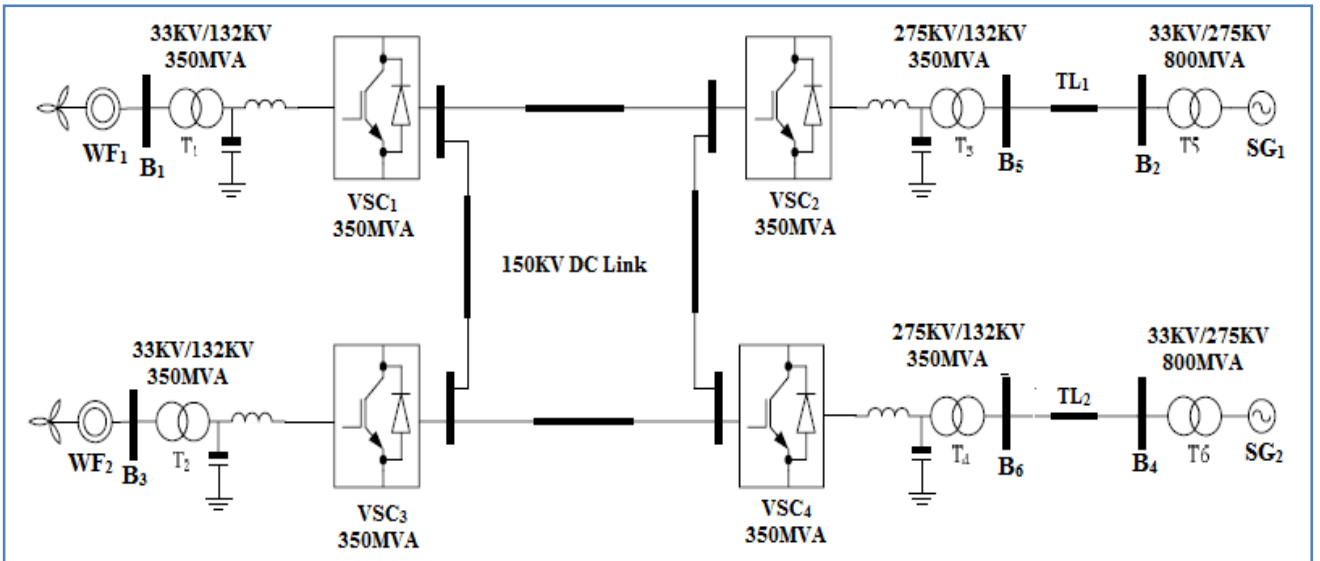
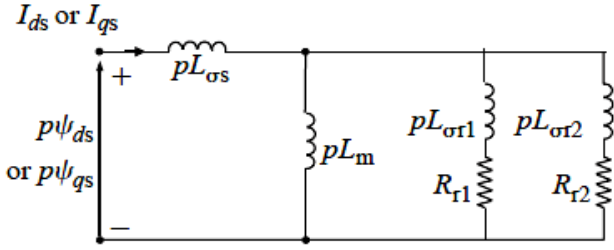
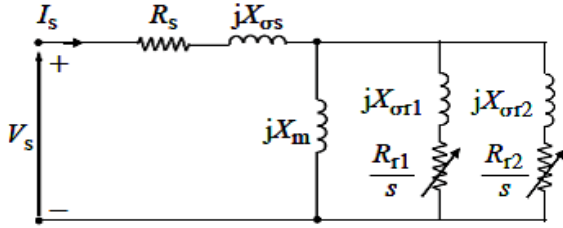


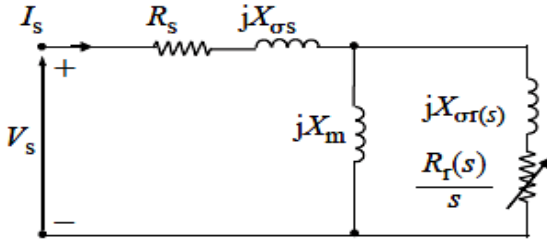
Fig. 1 Four-terminal dc transmission system based on voltage source connecting two offshore wind farms to the power network



(a) Operational equivalent circuit,



(b) Steady state equivalent circuit



(c) Circuit (b) with a single equivalent rotor branch

Fig. 2. Equivalent circuits of an induction machine with a double squirrel-cage or deep-bar rotor

Using $X(p) = \omega_s \psi_s / I_s$, the motor operational reactance can be written as

$$X(p) = (X_{os} + X_m) - \frac{C}{E} \quad (9)$$

where:

$$C = X_m^2 (R_{r1} + R_{r2})p + X_m^2 (X_{or1} + X_{or2})p^2$$

$$E = R_{r1}R_{r2} + [R_{r1}(X_{or2} + X_m) + R_{r2}(X_{or1} + X_m)]p + [X_{or1}X_m + X_{or2}(X_{or1} + X_m)]p^2$$

As in the case of synchronous machines, in order to derive the electrical parameters of the motor, it can be shown that Equation (9) can be rewritten as

$$X(p) = (X_{os} + X_m) \frac{1+(T_4+T_5)p+(T_4T_6)p^2}{1+(T_1+T_2)p+(T_1T_3)p^2} \quad (10)$$

where: $T_1 = \frac{X_{or1}+X_m}{R_{r1}}$, $T_2 = \frac{X_{or2}+X_m}{R_{r2}}$,

$$T_3 = \frac{1}{R_{r2}} \left(X_{or2} + \frac{1}{\frac{1}{X_{or1}} + \frac{1}{X_m}} \right), T_4 = \frac{1}{R_{r1}} \left(X_{or1} + \frac{1}{\frac{1}{X_{os}} + \frac{1}{X_m}} \right)$$

$$T_5 = \frac{1}{R_{r2}} \left(X_{or2} + \frac{1}{\frac{1}{X_{os}} + \frac{1}{X_m}} \right),$$

$$T_6 = \frac{1}{R_{r2}} \left(X_{or2} + \frac{1}{\frac{1}{X_{os}} + \frac{1}{X_{or1}} + \frac{1}{X_m}} \right)$$

Again, as in the case of synchronous machines, make use of an approximation that reflects practical double squirrel-cage rotor or deep-bar rotor designs. The winding resistance of the lower cage winding R_{r1} is much smaller than R_{r2} of the second cage winding nearer the rotor surface. This means that T_2 and T_3 are much smaller than T_1 and T_5 , and T_6 is much smaller than T_4 . Therefore, Equation (10) can be expressed in terms of factors as follows:

$$X(p) = (X_{os} + X_m) \frac{(1+pT')(1+pT'')}{(1+pT'_o)(1+pT''_o)} \quad (11)$$

where $T'_o = T_1$, $T''_o = T_3$ are the open-circuit transient and sub-transient time constants, and $T' = T_4$, $T'' = T_6$ are the short-circuit transient and sub-transient time constants.

The effective motor reactance at the instant of an external disturbance is defined as the sub-transient reactance X'' . Using Equation (11), this is given by

$$X'' = \lim_{p \rightarrow \infty} X(p) = (X_{os} + X_m) \frac{T'T''}{T'_oT''_o} \quad (12)$$

This can be written in terms of the motor reactance parameters as follows:

$$X'' = X_{os} + \frac{1}{\frac{1}{X_m} + \frac{1}{X_{or1}} + \frac{1}{X_{or2}}} \quad (13)$$

As in the case of synchronous machines, the second rotor cage is no longer effective at the end of the sub-transient period and the beginning of the transient period. Thus, using Equation 1 and 2, previously derived for the single rotor cage, obtained

$$X' = (X_{os} + X_m) \frac{T'}{T'_o} = X_{os} + \frac{1}{\frac{1}{X_m} + \frac{1}{X_{or1}}} \quad (14)$$

Using above Equations 12 and 14 for X' and X'' , is obtained the following useful relationship between the sub-transient and transient reactance and time constants

$$\frac{X''}{X'} = \frac{T''}{T'_o} \quad (15)$$

In order to determine the motor reactance under steady state conditions, recall that the rotor slip is equal to s and thus the angular frequency of the dq axes stator currents is $s\omega_s$. Therefore, the steady state motor impedance can be determined by putting $p = js\omega_s$ in $X(p)$ expression given in Equation 11. The induction machine operational reactance can be expressed from Equation 11 as a sum of partial fractions as follows:

$$\frac{1}{X(p)} = \frac{1}{(X_{os} + X_m)} \frac{(1+pT'_o)(1+pT''_o)}{(1+pT')(1+pT'')}$$

$$= \frac{T_0 T_0''}{(X_{os} + X_m) T' T''} \frac{(p + 1/T_0')(p + 1/T_0'')}{(p + 1/T')(p + 1/T'')} \quad (16)$$

which, using equations (12) for X'' and (14) for X' , can be written as

$$\frac{1}{X(p)} = \frac{1}{X_{os} + X_m} + \left(\frac{1}{X'} - \frac{1}{X_{os} + X_m} \right) \frac{p}{p + \frac{1}{T'}} + \left(\frac{1}{X''} - \frac{1}{X'} \right) \frac{p}{p + \frac{1}{T''}} \quad (16)$$

B. Induction Motor Behaviour under Short-circuit Faults and Modeling in the Sequence Reference Frame

Having derived the motor reactances and time constants, now able to proceed with analyzing the behaviour of the motor under three-phase short-circuit faults [2]. Using $X(p) = \omega_s \psi_s / I_s$ in Equation 3, the stator current is given by

$$I_s = \frac{\omega_s V_s}{X(p) [(p + j\omega_r) + \frac{\omega_s R_s}{X(p)}]} \quad (17)$$

As for synchronous machines, it can be made an assumption in the term $\omega_s R_s / X(p)$ to neglect the rotor resistances in the factors of $X(p)$ given in Equation 11. This is equivalent to setting infinite rotor time constants or neglecting the decay in the corresponding short-circuits currents, obtained $X(p) = X'$ which give

$$\frac{\omega_s R_s}{X(p)} = \frac{\omega_s R_s}{X'}$$

Also $X(p) = X''$ giving

$$\frac{\omega_s R_s}{X(p)} = \frac{\omega_s R_s}{X''}$$

Therefore, the armature or stator time constant T_a is defined as follows:

$$T_a = \begin{cases} \frac{X'}{\omega_s R_s} & \text{for a single rotor winding} \\ \frac{X''}{\omega_s R_s} & \text{for a double squirrel cage or deep bar rotor} \end{cases}$$

To simplify the mathematics, it is assumed that the motor is running at no load and hence the slip is very small and nearly equal to zero. Let the real instantaneous voltage, complex instantaneous voltage and complex phasor voltage values of the red phase stator voltage, just before the short circuit, be given by:

$$V_s(t) = \sqrt{2} V_{rms} \cos(\omega_s t + \theta_0) = \text{Real}[V_s(t)] \quad (18)$$

$$V_s(t) = \sqrt{2} V_{rms} e^{j(\omega_s t + \theta_0)} = V_s \quad (19)$$

$$V_s(t) = \sqrt{2} V_{rms} e^{j\theta_0} \quad (20)$$

where θ_0 is the initial phase angle that defines the instant of fault on the phase r voltage waveform at $t=0$. Neglecting stator resistance, i.e. letting $R_s = 0$, using equation $\omega_r = (1-s)\omega_s$ and putting $p=0$ in equation (17), obtain

$$I_s = \frac{V_s}{jX(p=0)(1-s)}$$

Using Equation 11, $X(p=0) = X_{os} + X_m$ and using Equation 19, the stator steady state current phasor is given by

$$I_s = \sqrt{2} I_{rms} e^{j(\theta_0 - \frac{\pi}{2})} \quad (21)$$

$$\text{where: } I_{rms} = \frac{V_{rms}}{(X_{os} + X_m)(1-s)}$$

Equation 21 shows that the current lags the voltage by 90° , as expected. Using the superposition principle, the total motor current after the application of the short circuit is the sum of the initial steady state current and the change in motor current due to the short circuit. The latter is obtained by applying a voltage source at the point of fault equal to but out of phase with the pre-fault voltage, i.e. $\Delta V_s = -\sqrt{2} V_{rms} e^{j\theta_0}$ Since the Laplace transform of ΔV_s is equal to

$$\frac{-\sqrt{2} V_{rms} e^{j\theta_0}}{p}$$

$$\text{And, } \frac{\omega_s R_s}{X(p)} = \frac{1}{T_a}$$

Obtaining from Equation (17)

$$\Delta I_s(p) = \frac{-\omega_s \sqrt{2} V_{rms} e^{j\theta_0}}{p [(p + \frac{1}{T_a}) + j\omega_r] X(p)} \quad (22)$$

Substituting the partial fractions Equation (16) for $X(p)$, obtained

$$\Delta I_s(p) = \frac{-\omega_s \sqrt{2} V_{rms} e^{j\theta_0}}{p(p + 1/T_a + j\omega_r)} \left[\frac{1}{X_{os} + X_m} + \left(\frac{1}{X'} - \frac{1}{X_{os} + X_m} \right) \left(\frac{p}{p + 1/T'} \right) + \frac{1}{X''} - \frac{1}{X' p + 1/T''} \right] \quad (23)$$

The complex instantaneous current $I_s(t)$ is obtained by taking the inverse Laplace transform of Equation 23. The total short-circuit current I_s (total) (t) is the sum of the pre-fault current given in Equation 21 and $I_s(t)$. The real instantaneous phase r stator short-circuit current is given by $i_r(t) = \text{Real}[I_s(\text{total}) e^{j\omega_r t}]$. For all practical purposes, $1/T_a$, $1/T'$, and $1/T''$ are negligible in comparison with ω_s and ω_r . Therefore, and after much mathematical operations, it can be shown that the total red-phase short-circuit current is given by:

$$i_r(t) \approx \frac{\sqrt{2} V_{rms}}{(1-s)} \left[\left(\frac{1}{X'} - \frac{1}{X_{os} + X_m} \right) e^{-t/T'} + \left(\frac{1}{X''} - \frac{1}{X'} \right) e^{-t/T''} \times \cos 1 - s \omega_s t + \theta_0 - \pi/2 - 2 V_{rms} 1 - s 1 X'' e^{-t T_s} \cos \theta_0 - \pi/2 \right] \quad (24)$$

which give :

$$\hat{i}(t) = \sqrt{2} I_{ac}(t) + I_{dc}(t) \quad (25)$$

The yellow and blue phases currents are obtained by replacing θ_0 with $(\theta_0 - 2\pi/3)$ and $(\theta_0 + 2\pi/3)$ respectively. The equations of sub-transient and transient reactances and time constants derived for induction motors can also be used for induction generator [2].

C. Modeling and control of VSC converter

i. VSC-HVDC grid-side converter

The equivalent circuit of VSC-HVDC grid side converter is shown in Fig. 3.

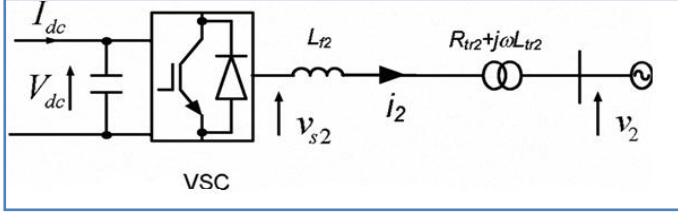


Fig. 3. Equivalent circuit of the VSC-HVDC grid side converter

The mathematical model based on the dq reference frame [4-6] is:

$$V_{sd2} = R_2 i_{d2} + l_2 \frac{di_{d2}}{dt} - \omega l_2 i_{q2} + V_{d2} \quad (26)$$

$$V_{sq2} = R_2 i_{q2} + l_2 \frac{di_{q2}}{dt} - \omega l_2 i_{d2} + V_{q2} \quad (27)$$

where, R_2 is the transformer resistance, l_2 is the inductance of the transformer plus interfacing reactor or $R_2 = R_{t2}$ & $l_2 = l_{t2} + l_{f2}$. If converter VSC₂ is assumed lossless, the power balance between its AC and DC sides can expressed as:

$$P_{d.c} = P_{a.c}(P_s + P_2) \quad (28)$$

$$V_{d.c} I_{d.c} = \frac{3}{2}(V_{sd2} i_{d2} + V_{sq2} i_{q2}) + CV_{dc} \frac{dV_{dc}}{dt} \quad (29)$$

So:

$$\frac{d}{dt} \begin{bmatrix} i_{d2} \\ i_{q2} \end{bmatrix} = \frac{1}{l_2} \begin{bmatrix} V_{sd2} - V_{d2} \\ V_{sq2} - V_{q2} \end{bmatrix} + \begin{bmatrix} -\frac{R_2}{l_2} & \omega \\ \omega & -\frac{R_2}{l_2} \end{bmatrix} \begin{bmatrix} i_{sd} \\ i_{sq} \end{bmatrix} \quad (30)$$

$$\frac{dV_{d.c}}{dt} = \frac{I_{d.c}}{c} - \frac{3}{2CV_{d.c}}(V_{sd2} i_{d2} + V_{sq2} i_{q2}) \quad (31)$$

When the voltage source converter is controlled using sinusoidal pulse width modulation (SPWM), the relationship between the modulation index M , DC link voltage $V_{d.c}$ and the dq components of the ac voltage at the converter terminal V_{sd2} and V_{sq2} are given by:

$$V_{sd2} = \frac{1}{2} M^* V_{d.c} \cos \delta \quad (32)$$

$$V_{sq2} = \frac{1}{2} M V_{d.c} \sin \delta \quad (33)$$

where, δ is a load angle.

The converter in Fig. 3 requires four independent control loops, the first and second loops are the current controllers that regulate the currents i_{d2} and i_{q2} ; the third control loop is the DC voltage controller that regulates the DC link voltage $V_{d.c}$; and the fourth loop is the AC voltage controller that regulates the AC voltage magnitude at the point of common coupling.

In order to design the current controller, the cross coupling terms in equations (30) & (31) are decoupled as follow:

$$V_{sd2} = U_{d2} - \omega l_2 i_{q2} + V_{d2} \quad (34)$$

$$V_{sq2} = U_{q2} - \omega l_2 i_{d2} + V_{q2} \quad (35)$$

$$U_{dq} = R_2 i_{dq2} + l_2 \frac{di_{dq2}}{dt} = K_{Pc}(i_{dq2}^* - i_{dq2}) + K_{ic} \int (i_{dq2}^* - i_{dq2}) dt \quad (36)$$

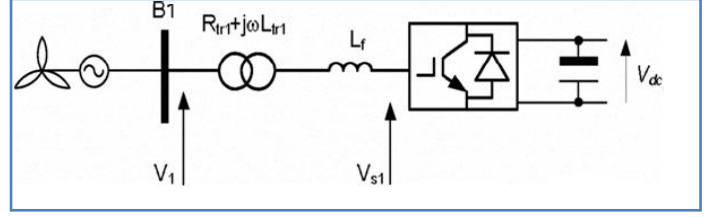


Fig. 4. Equivalent circuit of wind farm side converter

where K_{Pc} and K_{ic} are the proportional and integral gains of the current controller. Similarly, the DC link voltage and AC voltage controllers produce the set-points to the active and reactive current components i_{d2}^* and i_{q2}^* as given by:

$$i_{d2}^* = K_{P2}(V_{dc}^* - V_{dc}) + K_{i2} \int (V_{dc}^* - V_{dc}) dt \quad (37)$$

$$i_{q2}^* = K_{P3}(V_2^* - V_2) + K_{i3} \int (V_2^* - V_2) dt \quad (38)$$

where, $K_{P2}, K_{i2}, K_{P3}, K_{i3}$ are the proportional and integral gains of the dc voltage and ac voltage controllers respectively.

ii. VSC-HVDC wind farm side converter

As shown in Fig. 4 the schematic diagram of the wind farm side converter.

The mathematical model of the converter is based on the schematic of Fig. 4 the system on the ac side can be expressed in the dq reference fram as [4,5]:

$$V_{dq1} = R_1 i_{dq1} + l_1 \frac{di_{dq1}}{dt} + \omega l_1 i_{dq1} + V_{sdq1} \quad (39)$$

where $R_1 = R_{t1}$ and $l_1 = L_{t1} + L_f$

In order to transmit all the power generated by the wind farm to the grid without assigning a direct power command, the control system of the wind farm side converter (VSC) must be modified to maintain the voltage at bus B₁ at 1.0 p.u and guarantee the active power balance between the AC and DC sides of the converter VSC. Therefore, the reference active and reactive current components i_{d1}^* and i_{q1}^* are derived directly from the AC voltage loops as follow:

$$i_{dq1}^* = K_{PV}(V_{dq1}^* - V_{dq1}) + K_{iv} \int (V_{dq1}^* - V_{dq1}) dt \quad (40)$$

where K_{PV} and K_{iv} are the gains of the ac voltage controller that regulates the voltage at bus B₁.

iii. Shaft System Model

The large rotor inertia of the blades must be taken into account in controlling the speed. The acceleration and deceleration must be controlled to limit the dynamic mechanical stress on the rotor blades and the hub, and the electrical load on the generator and the power electronics. The instantaneous difference between the mechanical power produced by the blades and the electrical power delivered by the generator will change the rotor speed as follows [3].

$$J \frac{d}{dt} \omega = \frac{P_m - P_e}{\omega} \quad (41)$$

where: J = polar moment of inertia of the rotor; ω = angular speed of the rotor P_m = mechanical power produced by the blades; P_e = electrical power delivered by the generator. Integrating the above equation, yields:

$$\frac{1}{2}J. (\omega_2^2 - \omega_1^2) = \int_{t_1}^{t_2} (P_m - P_e). dt \quad (42)$$

The drive train of the wind turbine generator can be represented by a two-mass model as shown in Fig. 5, the first mass represents the blade, hub and low-speed shaft while the second mass represents high-speed shaft [7-11]. The relationship between the torque supplied by the wind turbine (T_{wt}), mechanical torque (T_m) and the electromagnetic torque developed by the generator (T_e) is given by [7]:

$$\begin{aligned} 2H_{\omega r} \frac{d\omega_r}{dt} &= T_{\omega t} - T_m \\ 2H_e \frac{d\omega_e}{dt} &= T_m - T_e \end{aligned} \quad (43)$$

which $T_m = D_m (\omega_r - \omega_e) + K_m \int (\omega_r - \omega_e) dt$

where H_{wt} , H_e , ω_r , ω_e , D_m , and K_m are wind turbine inertia, generator inertia, wind turbine rotational speed, generator rotational speed, mechanical damping constant and mechanical stiffness respectively.

The power extracted from the wind turbine can be controlled by adjusting the pitch angle (β) in case of over speed [6]. Conventional power plants normally have large inertia, this results in slow response to power change. For the fixed speed induction generator the Delta control approach is used and the wind farm is able to increase/decrease the generated power according to changes in the blade angle. When the wind farm generator senses any change in system demand, the induction generator speed will change resulting in activating the pitch angle controller and therefore the generated power will change to set system frequency [6].

4. SIMULATION RESULTS

In order to demonstrate of the proposed recovery strategy, in the case of symmetrical AC fault ride –through capability of the multi-terminal DC transmission system with a fault duration of 140 ms (7 cycles for 50 Hz) at $t=5$ s. As acknowledged, each wind turbine must be able to remain connected during ac fault for a period of 140 ms, the case study investigated.

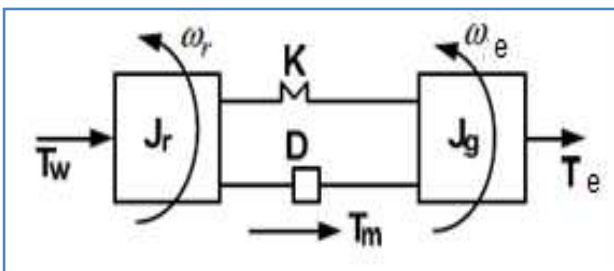
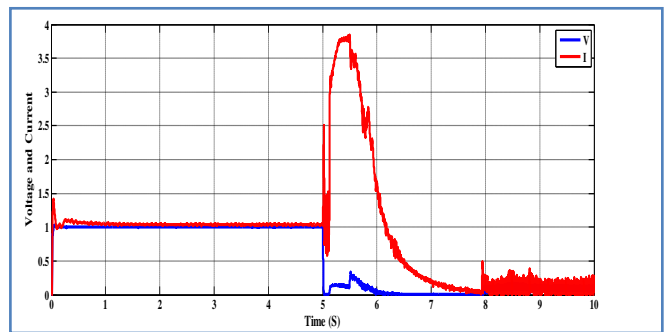


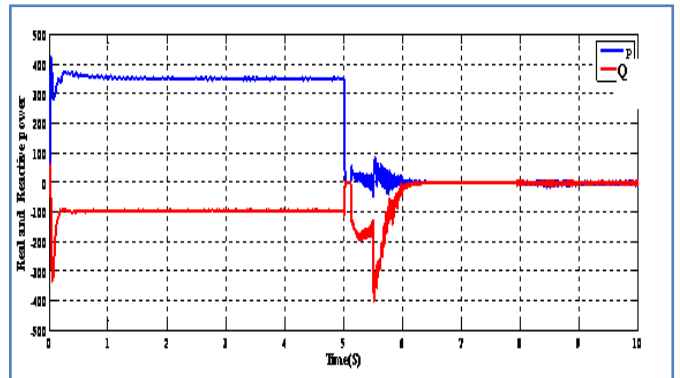
Fig. 5. Drive train (two-mass model)

A. Fault at Wind Side Station no. 1:

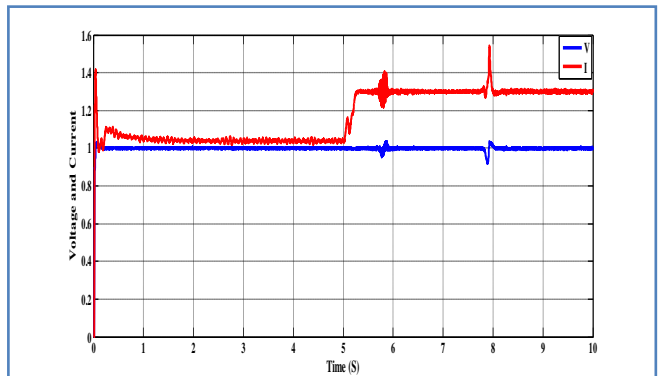
The system in Fig. 1 according to a case of three-phase fault at B_1 , the results obtained from case are shown in figures below. Fig. 6 (a and b) show that the voltage and active power of the wind station collapse to zero during the time of the fault, but another station of wind that is far away from the first one is less sensitive as in Fig. 6 (c and d). Although, for the AC fault on the wind side, from Fig. 6 (e and f) it can be noticed that, at the period of steady state stability voltage and power at the side of the power network is very sensitive toward any small disturbance at the wind side and they take long time to reach the steady state period, even with that far distance. The power curves and voltage curves at station 2 & 4 have similar behavior. In addition, from Fig. 6 (a and b) it is notice that the current at unit 1 take highest value 3.85pu before steady state period, but real power take small value 85.6 MW before it reaches zero at steady state period.



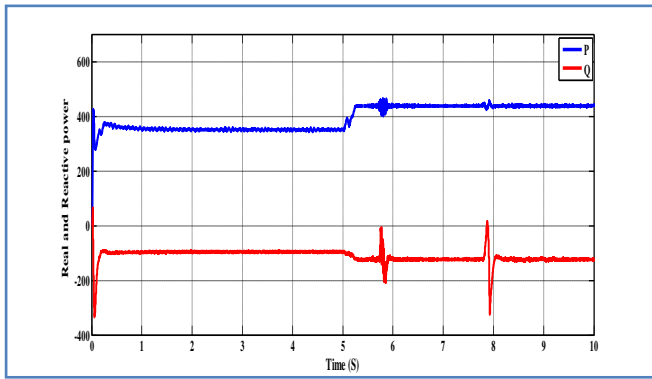
(a) Voltage and current at station no.1



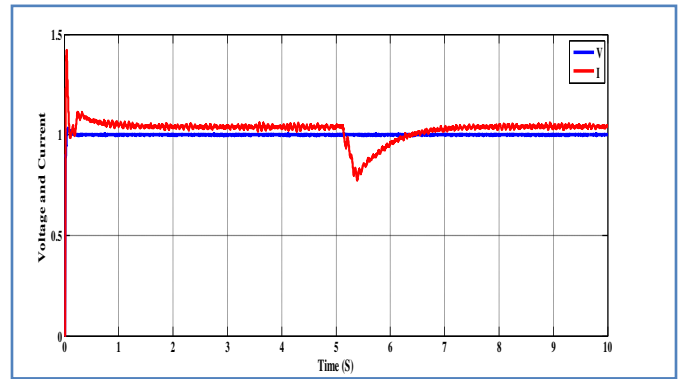
(b) Real and Reactive power at station no. 1



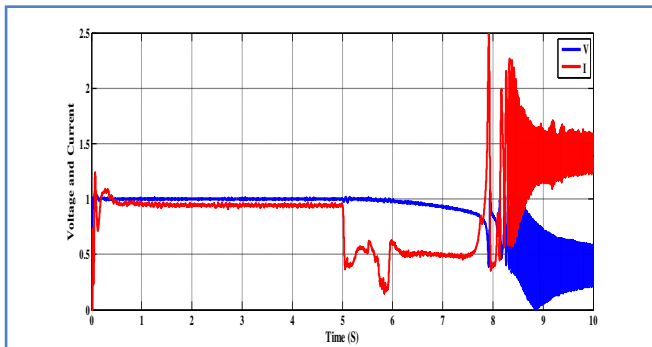
(c) Voltage and current at station no. 3



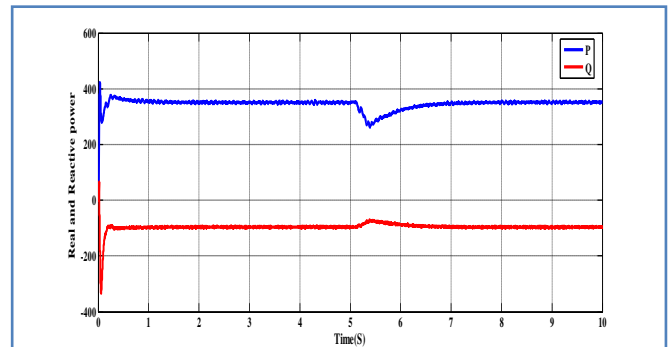
(d) Real and reactive power at station no. 3



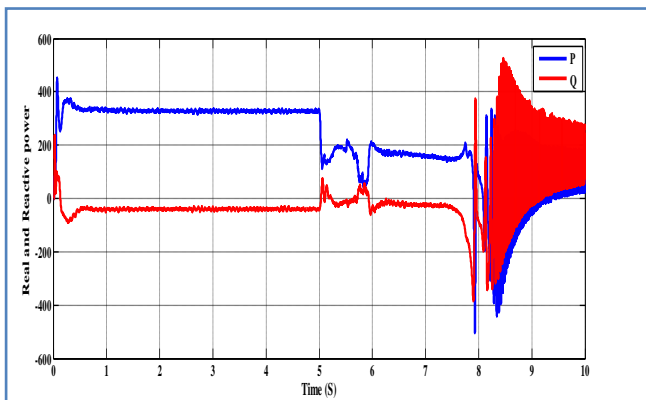
(a) Voltage and current at station no. 1



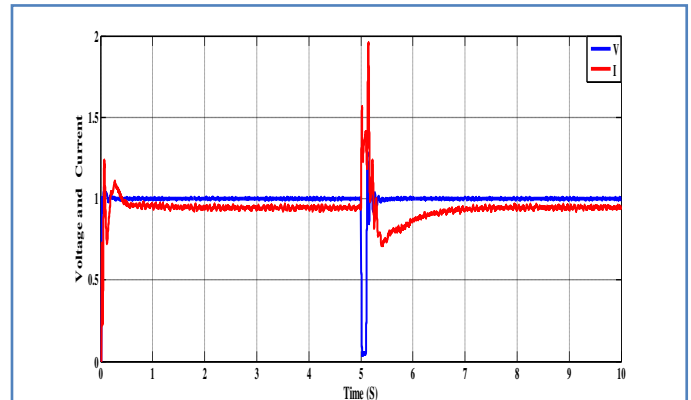
(e) Voltage and current at station no. 2



(b) Real and Reactive power at station no. 1



(f) Real and reactive power at station no. 2

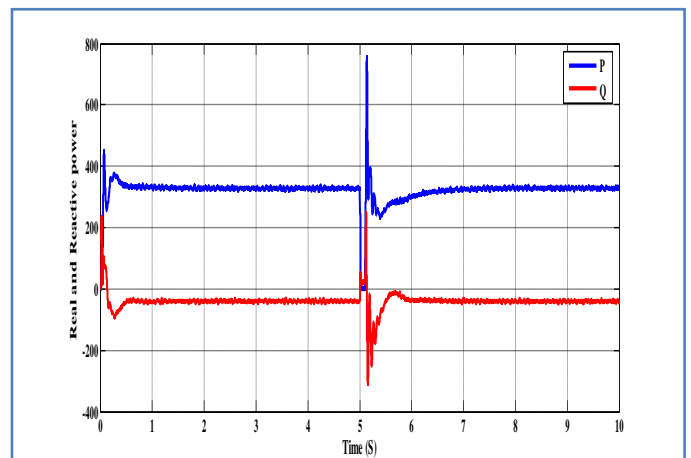


(c) Voltage and current at station no. 2

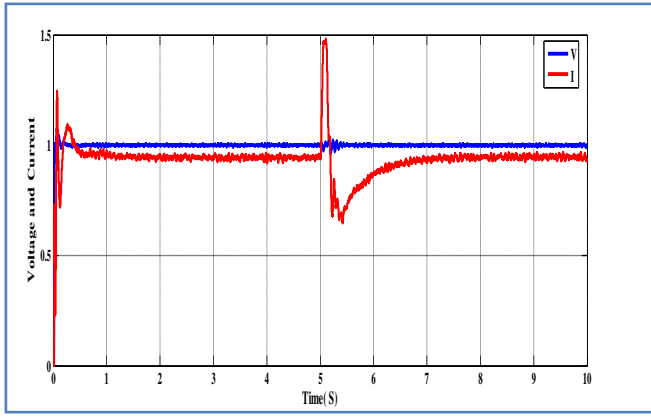
Fig. 6. Simulation Result for station no 1.

B. Fault at Power Network Side Station no 2:

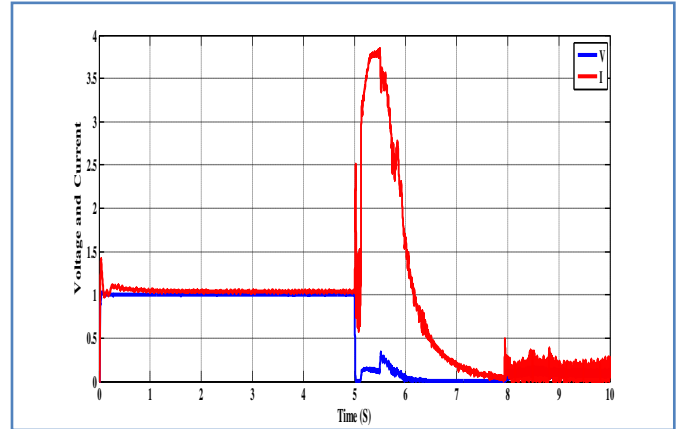
For the same system in Fig. 1 according to a case of the three-phase fault at B_2 , the results is given in Fig. 7 it can be observe in Fig. 7(a and b) that the voltage and active power at the wind farm side (busses B_1 , and busses B_3) remains less sensitive to the fault at the power network side, even with the wind farm side converter responding to the change in frequency in the power network. However, Fig. 7(e) shows that the dc link voltage of converter $VSC2$ increased during the fault period as a result of the trapped energy in the dc link. As expected as shown in Fig. 7(c and d), it can be noticed that the real power and voltage magnitude at bus B_2 collapses during the fault period as the reactive power capability of the converter decreases.



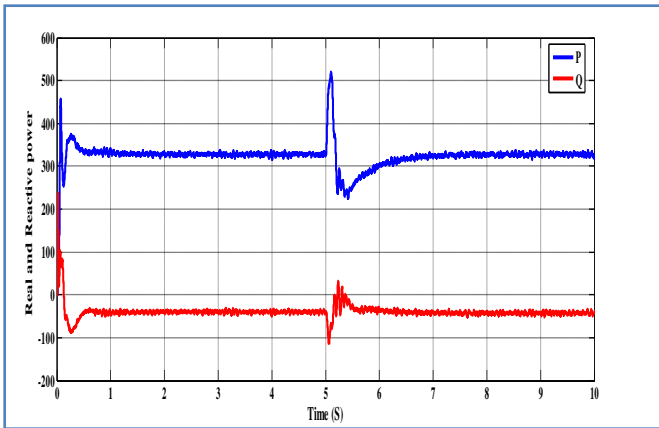
(d) Real and Reactive power at station no 2



(e) Voltage and current at station no 4

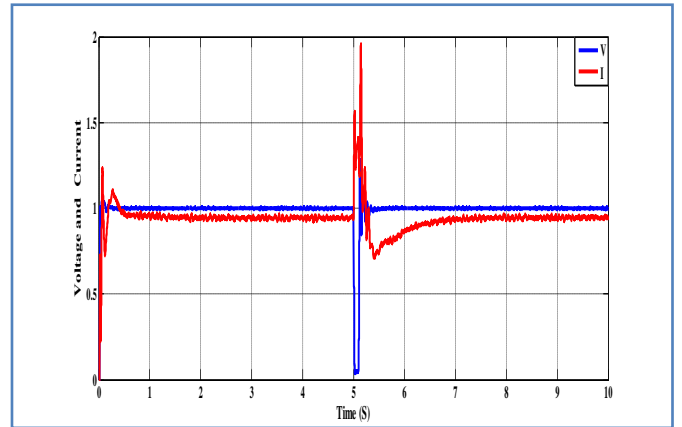


(a) Voltage and current at station no 1



(f) Real and Reactive power at MW-MVA at Station no 4

Fig. 7. Simulation results for scenario no. 2



(b) Voltage and current at station no 2

Fig. 8. Balanced three phase fault at wind side time and at grid side another time

Despite the voltage collapse at B_2 , the converter $VSC2$ contributes limited current to the fault. Moreover from Fig. 7(c and d) it can be noticed that the real power and current at station 2 take highest values $683MW$ and $1.57pu$ relatively before steady state stability.

C. Wind-side steady state condition

Induction generator (wind side) under short-circuit faults for the balanced three-phase fault has two components. The first term in Equation 18 is the ac component that consists of a sub-transient and a transient component which decay with time constants T' and T'' respectively. The second term is the dc component that has an initial magnitude that depends on θ_0 (phase angle) and it decays with a time constant T_a . Unlike a synchronous machine (grid side), there is no steady state ac component term and hence the short-circuit current decays to zero. In addition the frequency of the short-circuit current is slightly lower than the power frequency by the factor $(1-s)$ [2]. The curves of voltages and currents in Fig. 8 below explain the above mentioned findings.

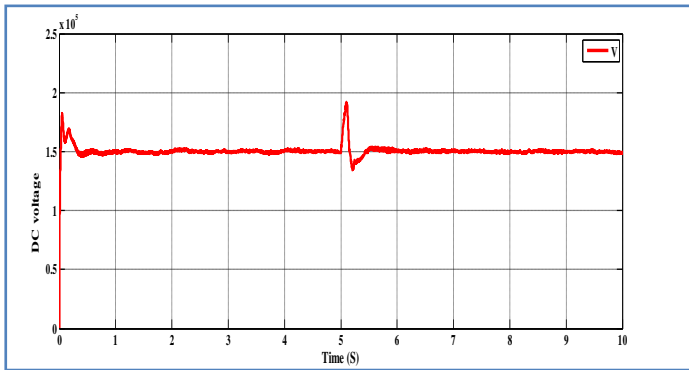
D. Comparison Between DC link and AC Voltage

Now, there are some comparisons between AC fault at wind side and AC fault at power network for DC link voltage and

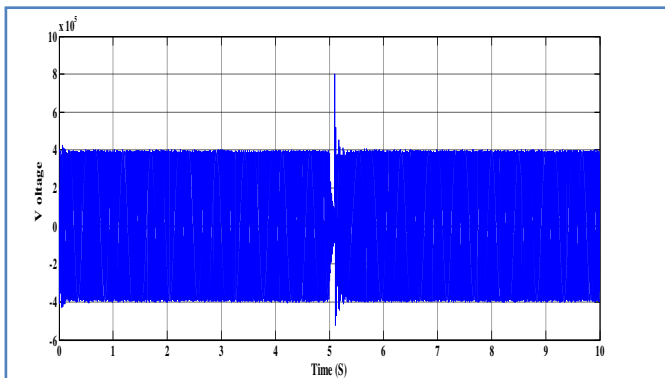
ac voltage. When the fault occurs in power network side stations the AC voltage collapses to zero during the time of the fault and return to its value when the fault is cleared, and the DC link voltage behave similarly as the ac voltage. However when the AC fault occurs in the wind side stations either for AC voltage or DC voltage the system behavior does not return to its normal operation after the fault is cleared. Figs. 9 and 10 show such behavior.

5. CONCLUSIONS

The voltage and active power at the wind farm side remains less sensitive to the three-phase fault at the power network side, even with the wind farm side converter responding to the change in frequency in the power network. Since power electronic converters are current control devices, they do not change significantly the fault level at the point of connection. In addition the introduction of voltage source converters $VSC-HVDC$ facilitates connection of weak systems such as wind farm, independently of the effective short circuit ratio ($ESCR$).

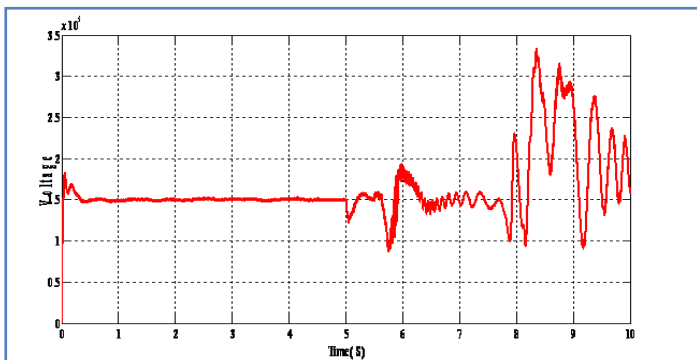


(a) The DC link voltage

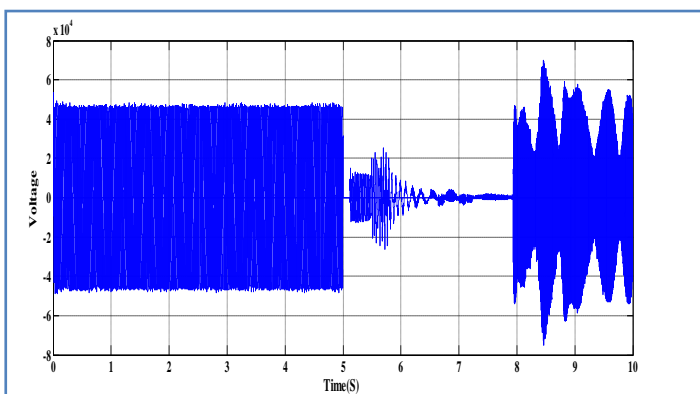


(b) AC voltage at station no. 2

Fig. 9. Fault in power network side



(a) The DC link voltage



(b) AC voltage at station no 1

Fig. 10. Fault in wind side

REFERENCES

- [1] Lie Xu , “The Role of Multi terminal HVDC for Wind Power Transmission and AC Network Support”, Queen’s University of Belfast, United Kingdom, 2010 IEEE.
- [2] Nasser D. Tleis, “Power Systems Modelling and Fault Analysis Theory and Practice”, Typeset by Charon Tec Ltd (A Macmillan Company); Chennai, India; First published 2008 ; pp 364-391.
- [3] M. R. Patul, “Wind and Solar Power Systems”, United States of America, 1999, pp 85 -121.
- [4] O. A. Giddani, G.P. Adam and O. Anaya-Lara, “Grid Integration of a Large Offshore Wind Farms Using VSC-HVDC in Parallel with an AC Submarine Cable”, Proceedings of the 44th International Universities Power Engineering Conference (UPEC), 1-4 Sept. 2009; pp 1 - 5.
- [5] O. A. Giddani, G.P. Adam and O. Anaya-Lara “Grid integration of Offshore Wind Farms using multi-terminal DC transmission systems (MTDC)”, 5th IET International Conference on Power Electronics, Machines and Drives (PEMD 2010);2010; pp 1 – 6.
- [6] O.A. Giddani, G.P. Adam and O. Anaya-Lara, G. Burt “Control Strategies of VSC-HVDC Transmission System for Wind Power Integration to Meet GB Grid Code Requirements”, International Symposium on Power Electronics Electrical Drives Automation and Motion (SPEEDAM); 14-16 June 2010 ; PP 385 – 390.
- [7] O. A. Giddani, G.P. Adam, O. Anaya-Lara and G. Burt Enhanced performance of FSIG wind farms for Grid Code compliance, International Symposium on Power Electronics Electrical Drives Automation and Motion (SPEEDAM); 14-16 June 2010.
- [8] Z. Yang, C. Shen, L. Zhang, M.L. Crow, and S. Atcity, “Integration of a STATCOM and battery energy storage”, IEEE Trans. Power System 2001.
- [9] K. Honghai, Wu Zhengqiu1, Z. Wenhui “Transient Stability of Multi-Machine Wind Turbine Generators System Connected to the Grid” International Conference on Energy and Environment Technology, 2009.
- [10] M.R.I. Sheikh, S.M. Muyeen, R. Takahashi, T. Murata and J. Tamura, “Transient stability enhancement of wind generator using superconducting magnetic energy storage unit,” Proceedings of the 2008 International Conference on Electrical Machines, 2008, IEEE.
- [11] S. Radha Krishna Reddy, J. S. Yam, A. S. Reddy “Wind Turbine Transient Stability Improvement in Power System Using PWM Technique and Fuzzy Controller” International Journal of Soft Computing and Engineering, Volume-3, Issue-1, March 2013.